AGU PUBLICATIONS

Geophysical Research Letters

RESEARCH LETTER
10.1002/2017GL076440

Key Points:
- Column water vapor has a bimodal distribution, defining moist-regime air masses revealed to be synoptic in scale, with sharp margins
- The margin of the moist regime meanders; morphed satellite data show where winds move the margin versus where they cross it while undergoing air mass transformation
- Maintenance of the moist regime and its sharp margins implies constraints on moist convection processes, which are shown to be erroneous in some current climate models

Correspondence to:
B. E. Mapes,
mapes@miami.edu

Citation:
Mapes, B. E., Chung, E. S., Hannah, W. M., Masunaga, H., Wimmers, A. J., & Velden, C. S. (2018). The meandering margin of the meteorological moist tropics. *Geophysical Research Letters*, *45*, 1177–1184. https://doi.org/10.1002/2017GL076440

Received 15 NOV 2017
Accepted 14 JAN 2018
Accepted article online 17 JAN 2018
Published online 30 JAN 2018

The Meandering Margin of the Meteorological Moist Tropics

Brian E. Mapes[1], Eui Seok Chung[1], Walter M. Hannah[2], Hirohiko Masunaga[3], Anthony J. Wimmers[4], and Christopher S. Velden[4]

[1]Rosenstiel School of Marine and Atmospheric Science, University of Miami, Coral Gables, FL, USA, [2]Program for Climate Model Development and Intercomparison, Lawrence Livermore National Laboratory, Livermore, CA, USA, [3]Institute for Space-Earth Environmental Research, Nagoya University, Nagoya, Japan, [4]Space Science and Engineering Center, University of Wisconsin–Madison, Madison, WI, USA

Abstract Bimodally distributed column water vapor (CWV) indicates a well-defined moist regime in the Tropics, above a margin value near 48 kg m^{-2} in current climate (about 80% of column saturation). Maps reveal this margin as a meandering, sinuous synoptic contour bounding broad plateaus of the moist regime. Within these plateaus, convective storms of distinctly smaller convective and mesoscales occur sporadically. Satellite data composites across the poleward most margin reveal its sharpness, despite the crude averaging: precipitation doubles within 100 km, marked by both enhancement and deepening of cloudiness. Transported patches and filaments of the moist regime cause consequential precipitation events within and beyond the Tropics. Distinguishing synoptic flows that *cross* the margin from flows that *move* the margin is made possible by a novel satellite-based Lagrangian CWV tendency estimate. Climate models do not reliably reproduce the observed bimodal distribution, so studying the moist mode's maintenance processes and the margin-zone air mass transformations, guided by the Lagrangian tendency product, might importantly constrain model moist process treatments.

Plain Language Summary Satellite snapshots indicate that tropical column-integrated water vapor (CWV) in the atmosphere has broad, almost-uniform moist regions, with sharp edges or margins that meander and move. This structure comprises a bimodal frequency distribution, an important qualitative distinction that justifies the term "regime." Deep convective storms and rainfall are largely confined inside the moist regime, where they are quite sporadic. In some places, the margin of the moist regime is observed to be moved by the wind, but in other places the wind flows across the margin, with air columns undergoing a rapid moistening as they cross the narrow marginal zone. The continued maintenance of this quasi-uniform vapor regime (despite spotty, intense losses in rain events), and of the sharpness of its margins, implies that convective and dynamical processes act in very concerted ways. We show that this concerted process coupling is nontrivial, since current climate models variously lack or exaggerate the bimodality of the CWV frequency distribution. A new data set for identifying regions of cross-margin flows (air column transformations) is offered.

1. Introduction

Tropical meteorology is arguably defined by moisture (reviewed for instance in Sherwood et al., 2010), even more than by the weakness of the Coriolis force at low latitudes. Much of the geographical Tropics is covered by marine deserts, where water evaporated from warm seas is lofted by cumulus clouds to be carried away on the wind to concentrated precipitation events in the wet climates defining the "deep" tropics. Even there, rain events are sporadic and localized, but their occurrence can be strongly statistically bounded. For instance, monthly precipitation over the tropical ocean requires sea surface temperature (SST) above a "threshold" (Graham & Barnett, 1987, Johnson & Xie, 2010).

Time-resolved data help refine these statistical climate constraints: *instantaneous, local* precipitation is sharply contingent on simultaneous column water vapor (CWV; Bretherton et al., 2004, Neelin et al., 2009, Schiro et al., 2016). This steep dependence fits the physics paradigm of self-organized criticality in carefully rescaled logarithmic statistics (Peters & Neelin, 2006). At first blush, a vapor-rain relationship may sound almost tautological, since rain-producing clouds are themselves columns of saturated air. But the residence time of water vapor is a week or more, set by Earth's temperature and surface pressure (and thus an atmospheric vapor

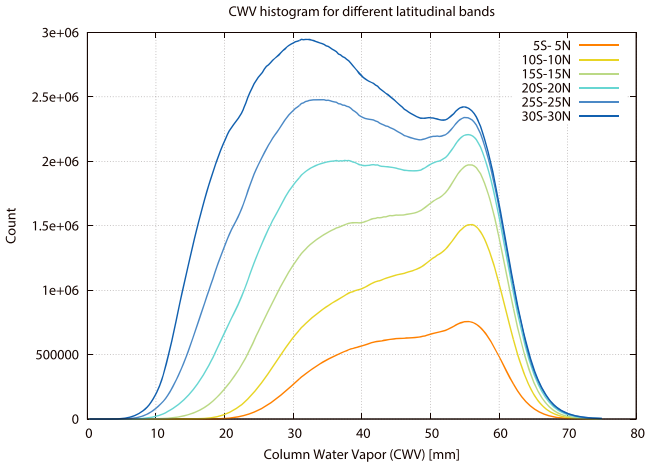

Figure 1. Histograms of instantaneous CWV estimates over the oceans. Microwave satellite measurements on approximately 25 km footprints are considered reliable within 1 mm. Nested latitude belts are indicated with colors. The minimum at 48 mm over the geographical tropics (blue curves) defines our titular "margin" of the moist tropics.

capacity of a few cm liquid equivalent) and by the few mm d^{-1} (order 10^2 W m^{-2}) vigor of its energy-water cycle. This fairly long residence time offers hope but no guarantee of commensurate multiday coherence and predictability of *features* in the vapor field.

Space-time precipitation data further refine the view but reveal a bewilderingly broad spectrum of disturbances, right down to local triggering of updrafts in the metastable tropical atmosphere (Schultz et al., 2000). However, a smooth synoptic spatial scale can undeniably be glimpsed in the water vapor field, as sampled by passive microwave sensors on a constellation of polar-orbiting satellites since the 1990s. Unfortunately, the narrow swaths intermittently sampled from multiple platforms do not immediately reveal a lucid spatial and temporal view. Since 2010, a data processing technique called "morphing" (or morphological compositing) has addressed this challenge, taking into account the main form of time evolution in the CWV field between sampled swaths: horizontal advection by lower tropospheric winds (Wimmers & Velden, 2011; see section 6). This morphing analysis has been implemented on the near real-time data stream and yields false-color animations that are highly valued by forecasters. Inspired by insights from those animations, in May 2014 we devised quantitative diagnostic outputs from the morphing scheme (see section 6) that spotlight the nonadvective tendency terms in the 2-D CWV field's time evolution. Below we show some first looks at those tendencies, whose meaning lies in the context of a steep-sided plateau structure observed in the CWV field itself.

2. Linking CWV Distributions to Space-Time Structure

The frequency distribution of CWV observed over the oceanic Tropics exhibits a distinctive bimodal structure (Figure 1), with a clear minimum near 48 mm and a relatively sharp peak centered near 55 mm. This result should be carefully distinguished from the bimodality of *upper level* vapor, which was shown by Zhang et al. (2003) to spring from its very short residence time. There, sporadic injections by convection from below leave most of the humidity values to accumulate in a dry mode, bounded below by the physical constraint of positivity. In contrast, Figure 1 is the long-lived column vapor field, and we emphasize its moist mode. We shall see that the present result implies that convective + dynamical processes are conspiring to play a concerted maintenance role, not just a stochastic source role in the presence of a rapid decay.

Daily averaged data do not resolve the frequency minimum (Bretherton et al., 2004) but still show a fairly sharp shoulder at the upper end of the distribution. Rescaling by an air temperature-dependent saturation value (differing by about 2 K from the warm Indo-Pacific to the cooler Atlantic) sharpens the distribution structure (Neelin et al., 2009; Peters & Neelin, 2006) and is a more fundamental quantity for study under climate changes. Here the minimally processed and direct CWV observations suffice and have the virtue of simplicity.

Spatial maps of CWV and precipitation, 11 days apart, are shown in Figure 2. The CWV measurement is most reliable against the low-emissivity backdrop of water, so land areas are masked. The nighttime scenes depicted here (00 UTC nominal hour) have relatively minimal precipitation over land. The 48 mm contour (black) clearly confines almost all the precipitation, which appears quasi-randomly arrayed within that, in the form of mesoscale (100 s of km) convective systems (Houze 2004). The western Indian Ocean basin is an especially interesting region for these moisture dynamics: Islands and filaments of moist, sporadically precipitating air masses are seen to drift for considerable periods in the weak, recirculating basin-scale flow, in all seasons. The longevity of these air masses begs the question of their maintenance mechanisms, and their landfalls are consequential for the semiarid and arid adjacent lands. Cyclones transiting into the midlatitudes sometimes remove significant areas of the moist-mode air mass, as suggested in the Southern Hemisphere of Figure 2b. Meanwhile, its area is replenished by both local regrowth processes within the Indian basin and transport from the east (clear in MIMIC-TPW animations online).

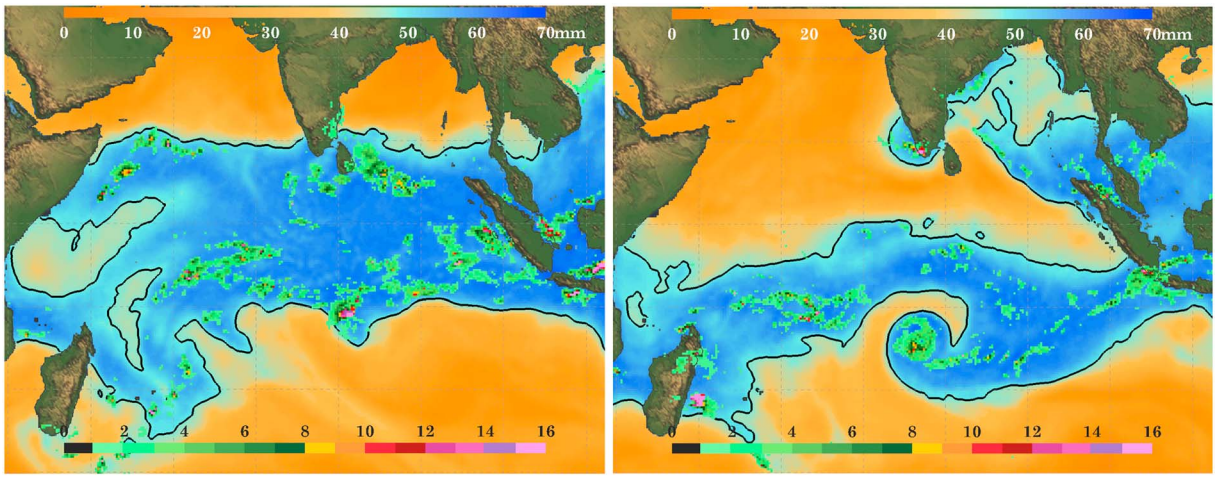

Figure 2. Multisatellite blended CWV data (Wimmers & Velden, 2011; top color legend and black 48 mm contour, masked over land where measurements are unreliable), overlain with rainrate estimated by the TRMM 3B42 product (Huffman et al., 2007; bottom color legend in mm/d units), for 20 December 2011 (left) and 31 December 2011 (right) at 00 UTC, at contrasting phases of an intraseasonal oscillation.

3. Mean Structure of the Margin Zone

To reveal more about the sharp spatial structure of the margin, Figure 3 shows the north-south structure of composite averages of 3 years of satellite data products, centered on the most poleward 48 mm CWV value in each swath, combining both Northern and Southern Hemispheres. This poleward edge is the easiest aspect of the meandering margin to find and isolate algorithmically, and latitude is a convenient grid coordinate for composite construction, but the folded contour in Figure 2b shows its imperfection in some cases. Despite this crude data averaging, the margin is still seen to be a relatively sharp front of approximately (100 km) scale, separating subtropical from tropical regimes that are broadly different across approximately (1,000 km) scales. CloudSat radar echo coverage (clouds and rain, top panel) increases by at least 50% over 100 km at low levels. Sloping contours indicate a deepening of low clouds into the middle troposphere over this distance, while high clouds overhang the subtropics at right by a few hundred km, sometimes obscuring

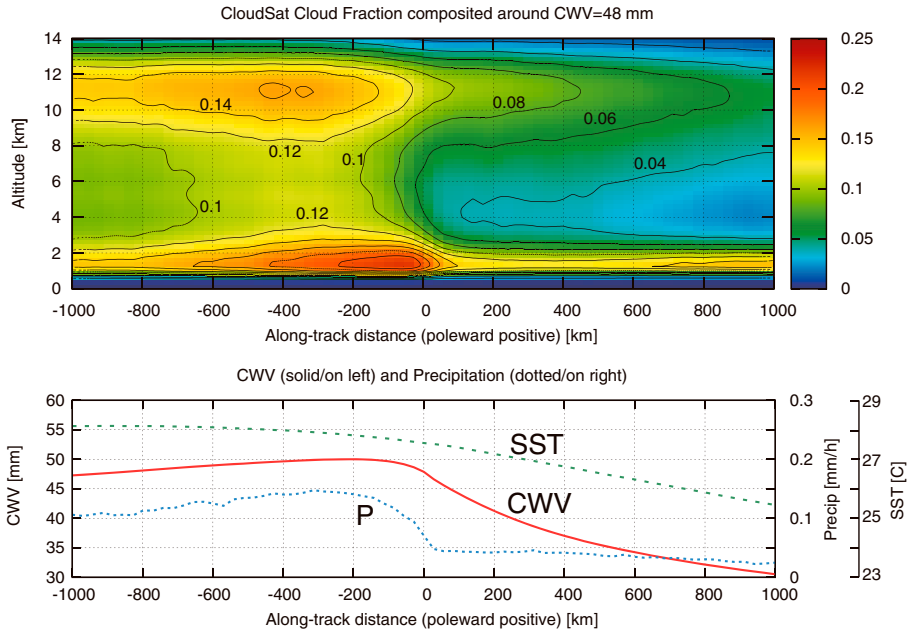

Figure 3. Composite of A-train (Stephens et al., 2002) satellite data around the most poleward 48 mm value in each north-south grid swath. Top: Echo fraction detected by CloudSat radar is shaded and contoured. Bottom: CWV (mm), precipitation rate *P* (mm/h), and SST (C) estimated from AMSR-E microwave emission data by Remote Sensing Systems (remss.com).

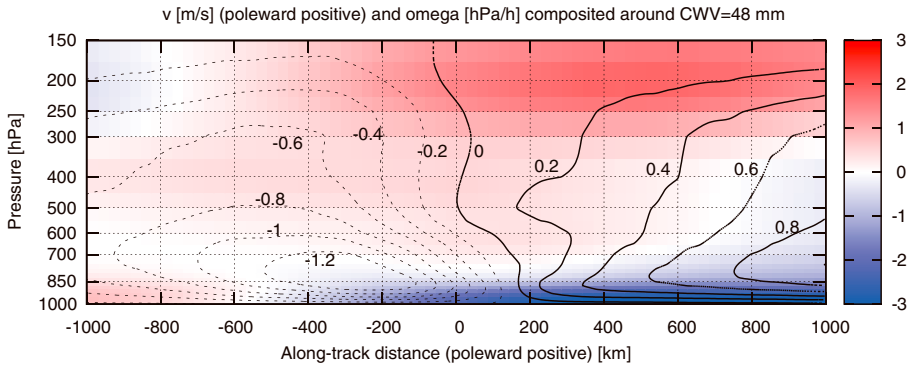

Figure 4. Composite of analyzed air velocity fields, as in Figure 3. Poleward wind is color shaded, while vertical wind is contoured. Negative contours indicate upward motion on this hydrostatic pressure coordinate.

visible and infrared satellite views. Microwave data (lower panel) are insensitive to clouds and reveal that mean precipitation jumps very sharply, doubling or even tripling across the origin. The steepness of the CWV curve near the origin is another manifestation of the distributional minimum from Figure 1. Sea surface temperature (SST), however, exhibits only a smooth latitudinal gradient in this average, since it does not follow nor anchor the daily meanderings of the margin. While the SST value of 27.5°C at the origin is consistent with scatterplots of monthly mean climate data (Graham & Barnett, 1987; Johnson & Xie, 2010), the CWV front is seen to meander from day to day with the weather (Figure 2).

Composite structure in vertical and poleward wind components estimated by the ERA-Interim reanalysis (Dee et al., 2011) are presented in Figure 4. Upward motion (negative values of the contoured field) exhibits an equatorward slope with height in the lower troposphere over the approximately 200 km scale of the composite border zone (near the data's resolution limit). The main poleward flow is near 200 hPa, but slight secondary poleward flows can be discerned in the middle troposphere. These data are less fundamentally observational than the satellite observations of Figure 3, however, so the details may not be entirely trustworthy (Zhang et al., 2008).

4. Air mass Transformations Versus Moving the Margin

Does the wind blow the margin, or blow through it? The answer must include both. Animations of the margin's meanders and excursions (web-search MIMIC TPW) make clear that these are largely pushed by winds from day to day. But winds must cross the margin too, because otherwise the convergence of flow in the moisture-bearing lower troposphere would collapse the moist region to infinitesimal size. The sharpness of the margin suggests that air columns undergo a relatively rapid moistening process as they cross it. Since moistening rates exceeds surface evaporation, horizontal convergence (or equivalently, vertical advection) of moisture must be involved, perhaps as a response to bottom-heavy convective heating while temperature gradients remain weak (e.g., Chikira, 2014), translating to a negative value of gross moist stability (e.g., Raymond et al., 2009).

Dispersion of the column integral by sheared winds make the concept of "air columns" rather loose, but that is precisely what makes the mode-and-margin structure of CWV interesting: the column integral of an unmaintained passive tracer with a broad surface source, several km depth, and a residence time of a week would not exhibit such structure.

Figure 5 shows this study's novel diagnostic for distinguishing margin-crossing air masses: the Lagrangian CWV Tendency (LCT in the nomenclature of Hannah et al., 2016). Here we estimate this LCT as an analysis tendency (AT) within the data assimilation process that morphing embodies: It is *the tendency required to explain how the evolution observed in the satellite data differs from that predicted by a horizontal advection-only procedure* (see section 6 for more details). In the moisture budget, LCT represents the sum of all nonhorizontal-advection terms: surface evaporation, plus the *sum* of cloud processes and vertical advection, called "column process" by Chikira (2014). Because the radically spotty vapor sink of precipitation is closely compensated by vertical advection by the equally spotty upward motion induced by the associated latent heat release, this

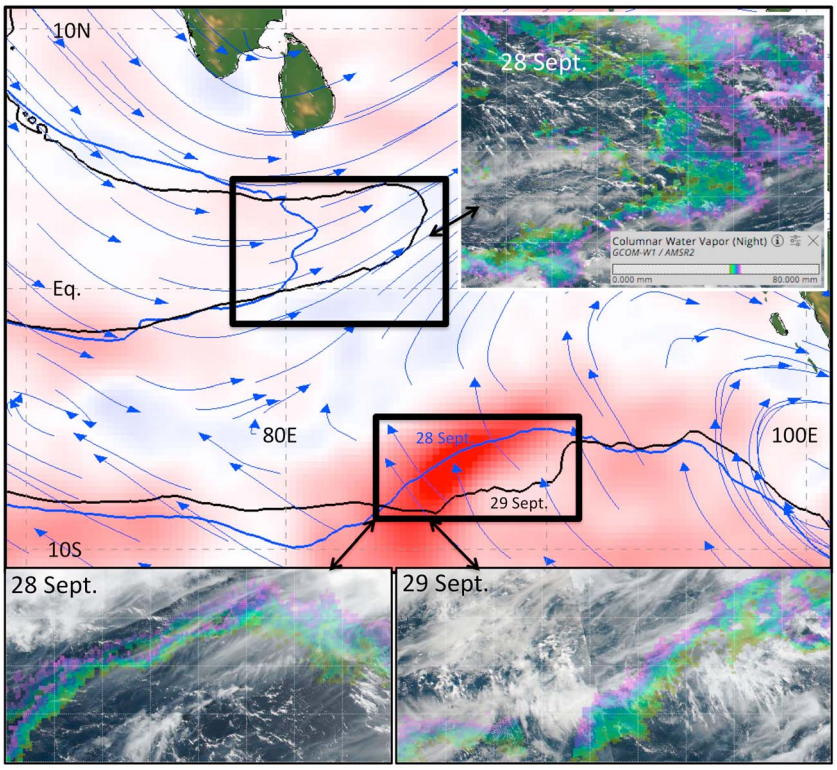

Figure 5. CWV (blue 48 mm contour) and daily-mean Lagrangian tendency (shading; red maximum is 5 mm/d) for 28 September 2016. The black contour is CWV 1 day later, on 29 September. Blue curved arrows show 1 day trajectories of 850 hPa winds over the day, computed from MERRA-2 reanalysis. Inset images corresponding to the black boxes show the visible character of cloud fields on the indicated days, from Suomi NPP VIIRS, overlaid with the 46–50 mm CWV range from GCOM-W1/AMSR2 in transparent colors (color bar in upper right inset). These cloud and vapor images can be reproduced exactly, interacted with, and expanded to other locations and times at https://go.nasa.gov/2EPmqh2.

direct observation of their sum is a valuable quantity that cannot be reliably constructed from individual estimates of those subcomponents. Here we display a daily mean AT, because intersatellite calibration differences cause unphysical AT signals in this merged product from multiple sun-synchronous satellites, which vanish in the daily average.

In Figure 5, strong positive values of LCT on 28 September 2016 (dark red shading at bottom), indicative of air columns undergoing strong moistening, are seen to occur near the margin (blue and black contours are CWV = 48 mm on 28 and 29 September, respectively). Indeed, the 48 mm contour is seen to have migrated *south* with time, even though the 850 hPa winds were northward. Bands of positive LCT are also seen in the west, straddling the moist belt from 2S to 8S, maintaining its width over the day despite convergent north-south inflowing winds. Meanwhile, along the equator, LCT is small, and correspondingly the 48 mm contour moved eastward in a day (blue to black) more than half the length of the 1 day 850 hPa wind trajectories (curved arrows).

Cloud images for the boxed areas in Figure 5 allow a glimpse of the hypothesis that bottom-heavy heating in shallow precipitating convection is active in strong LCT events. In both boxes, cloud streaks support the general correctness of the analyzed low-level wind direction, and the position and movement of the 48 mm margin (rainbow colorations). Along the equator, where dry air is sweeping eastward with time, the shallow cumulus fields are modest in coverage. In contrast, in the strong-LCT box to the south, vigorous convection is seen near the rainbow-colored margin zone, especially on 29 September. The difference emphasizes that there are many flavors of moist convection (Stevens, 2005). The cloud fields in Figure 5 are consistent with our process hypothesis, at least in this rather arbitrary sample, selected as the most illustrative day in the Indian Ocean in the first month of the AT data we have examined in this way. Causality remains unclear: Did forced (adiabatic) ascent moisten and cool the air columns by advection, leading to the vigorous convective development seen at lower right on 29 September? Or did convection there

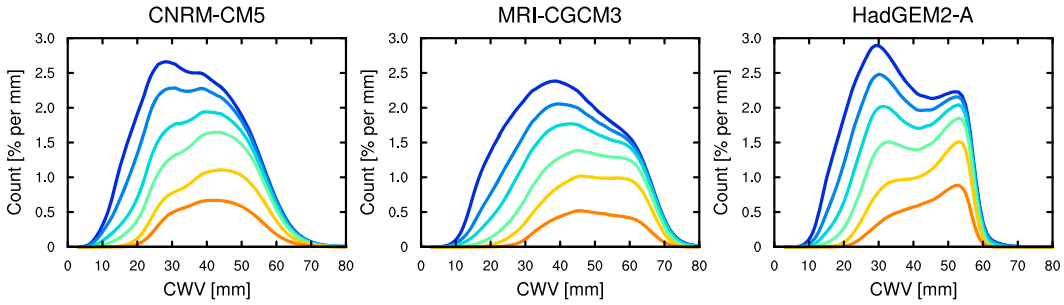

Figure 6. Column water vapor frequency distributions like Figure 1 in 3-hourly data from three uncoupled atmospheric models in the Climate Model Intercomparison Project archive (Taylor et al., 2012).

induce vertical advection by its latent heating? Finer temporal discernment will be required, but with these AT fields as a guide it should be possible to build more incisive, statistically significant characterizations of the convective weather of the margin zone.

We interpret the AT field in most locations as an estimate of LCT, although perusal suggests it still has some data artifacts. While these are easily discerned by eye (as satellite swath- and sweep-shaped patches), they are not trivial to remove by algorithm, so blind averaging of this data set (version 4) should be avoided until more robust screening methods are developed. Two years of AT data are available in our repository, at this writing, and another 1.5 years are being processed.

5. Summary and Discussion

We showed that moist air masses in the maritime Tropics comprise a distinct atmospheric regime (i.e., a mode of the CWV frequency distribution), with sharp margins (a minimum, Figure 1). An associated steep statistical gradient of average rainrate with CWV (variously called a "transition," "onset," or "pickup" in the literature) is a jump in the probability of sporadic but intense convectively driven rains, including the associated stratiform (Houze 1997) component (Ahmed & Schumacher, 2015). Animated maps clarify that the sharp statistical gradient is spatially synoptic and temporally coherent over days, in the form of many-degree-scale plateaus (Figure 2) whose edge fronts are as narrow as 100 km even in highly averaged observations (Figures 3 and 4).

Air columns crossing into the tropical plateau of high CWV sometimes undergo rapid moistening but in other situations winds move the position of the margin (Figure 5). The large-scale flow or thermodynamic profiles that cause these different situations remain unknown. Vigorous but shallow precipitating convection, whose bottom-heavy heating profile can drive efficient column moistening (e.g., Chikira, 2014; Mapes, 2001; Raymond et al., 2009), appears to be implicated in the air mass transformation process. Fields from initialized global weather models may clarify if those models can reproduce these processes, or at least if their analyzed thermodynamic and dynamic environments are appropriately different between advected versus crossed segments of the moisture margin (even if their convection schemes fail to distinguish the shallow-deep convection spectrum properly). A related but distinct question is: how are the plateau CWV values maintained in the face of a spotty precipitation sink? Again, the sum of precipitation and advection by latent heating-coupled updrafts (Chikira's "column process") is certainly involved, but the causality needs elaboration.

These processes present an incisive, holistic test of the intimately interacting profiles of lapse rate, vapor, subgrid moist processes, and divergent flow response to bursts of latent heating. Figure 6 indicates that contemporary climate models can indeed fail or succeed at this test, in diverse ways, making this an incisive example of a "process-oriented diagnostic" (Kim et al., 2014) or perhaps even an "emergent constraint" (Allen & Ingram, 2002).

Conditional sampling of cloud scenes based on LCT and/or CWV plateau geometry will further illuminate these mechanisms and sharpen the associated modeling constraint. Like any fundamental local features of nature, these sharp but meandering margins invite reconsiderations of all averaging-blurred low-frequency envelope dynamics in the moist tropics, from intraseasonal variability to greenhouse warming. Do large-scale tropical moisture changes occur via simple right-left shifts of the CWV frequency distribution? Or might they instead involve changes in the distribution; that is, changes in the *area* of the moist plateau (mode), for

instance due to changes in synoptic eddies that sculpt and erode it, as evoked by Figure 2? How might global warming-driven widening of the dynamical tropics (Seidel et al., 2007) affect the synoptic export of tropical moist air masses (Allen & Mapes, 2017; Knippertz et al., 2013), with implications in the tropics as well as in the receiving latitudes (e.g., Shields & Kiehl, 2016)? Feature analysis, not just field analysis, may be needed to address such questions. In addition to somewhat arbitrarily defined entities such as the popular "atmospheric rivers," we suggest that geophysically fundamental features with parsimonious definitions (like a bimodal distribution's internal minimum) should also be targets of such research.

Observationally, robust and cloud-insensitive retrieval of CWV over the complex emission backdrop of land remains a frontier. As the challenges are met, morphing approaches may become applicable across the coastline. Experimental morphed CWV products over land are now available (http://tropic.ssec.wisc.edu/real-time/mtpw2), but the land fields are much less coherent in appearance than over water (whether rightly or wrongly). The "ingredients" of convective activity over land are more diverse and more variable (Doswell et al., 1996), so CWV is likely less determinative and may also occur in less coherent and uniform patches, as its evaporative source is also more heterogeneous. At some stage, output grids from well-calibrated weather models assimilating diverse data sets through long time windows may surpass raw data and simpler techniques like morphing. But at present, lessons accessible from these fairly direct observations and a light touch of modeling (horizontal time-to-space conversion only) remain to be revealed and understood.

6. Methods

Data used in Figure 3, the composite around the 48 mm "margin" of Figure 3, are from the A-Train of satellites (Stephens et al., 2002) with local overpass times of 1:30 (a.m. and p.m.), covering the period July 2006 through December 2009. The CloudSat 2B-GEOPROF (Marchand et al., 2008) product in Figure 3 was provided by the CloudSat Data Processing Center (www.cloudsat.cira.colostate.edu). The AMSR-E retrievals of CWV, precipitation, and SST, masked over water only, were obtained from Remote Sensing Systems (remss.com). All satellite data were resampled onto a 0.25° latitude-longitude grid before processing. Circulation data in Figure 4 are from the ERA-Interim reanalysis (Dee et al., 2011), interpolated linearly to the satellite data's grid mesh and overpass time from 6-hourly data. Data were used over 25°S–25°N only, so the poleward most 48 mm value omits any possible high CWV values poleward of 25° latitude. Precipitation estimates on Figure 2 are from the TRMM 3B42 product (Huffman et al. 2007).

The morphed (MIMIC-TPW) CWV product in Figures 2 and 5 (Wimmers & Velden, 2011) uses an older water vapor retrieval than the AMSR-E results in Figure 3, with some clipping of high values, but values are similar within a very few mm. The analysis tendencies in Figure 5 are a new (since May 2014) by-product of MIMIC-TPW's construction. In the MIMIC process, CWV swath data from multiple satellites have their pixels translated in a time-to-space conversion exercise, according a specified two-dimensional vector wind field (a layer-averaged wind from 1,000 to 700 hPa from the GFS weather forecast model, detailed in Wimmers & Velden, 2011). At each product definition hour, in each spatial grid cell, the nearest-in-time translated observations at that location are averaged to produce the CWV product (colored in Figure 2 and contoured on Figure 5).

The new Analysis Tendency (AT) field (colored in Figure 5) is derived as the *difference* of these same two nearest-in-time values at each location, divided by the difference between the observation times. This AT measures the deviation of the observations from the first guess by a model that solves the horizontal advection equation. If the data and horizontal advection procedure are correct, the AT therefore represents the sum of all the other terms in the CWV budget: a quantity called (horizontally) Lagrangian CWV tendency (LCT) by Hannah et al. (2016). LCT equals surface evaporation minus precipitation plus vertical advection. AT is thus LCT plus all errors in the data and in the advection procedure. Data errors include swath-shaped stripes due to intersatellite calibration differences, which vanish upon daily averaging since orbits are sun-synchronous, and occasional swath-shaped outliers in the AT distribution of uncertain origin that we have clipped before daily averaging. Errors in the advecting velocity show up as AT dipoles across CWV gradients, especially in places where temporal "jumps" of features are seen occasionally in the MIMIC-TPW animations. Visually, we see only mild and rare evidence of this fingerprint of advection errors, so the daily mean AT product is interpreted in Figure 5 as being almost equal to LCT.

Model data in Figure 6 are from the CMIP-5 archive (Taylor et al., 2012) and were downloaded from the Earth System Grid Federation server (https://esgf-node.llnl.gov/projects/esgf-llnl/). The models shown (CNRM-CM5,

HadGEM2-A, and MRI-CGCM3) were arbitrarily selected as the first three we found with availability of 3-hourly outputs of CWV. The distributions are shown for 1 year (2008s prescribed observed SST and sea ice conditions).

Acknowledgments
This work was supported by award NA13OAR4310156 from NOAA, U.S. Department of Commerce, and by NASA-NEWS program grant NNX15AD11G. W. M. H.'s work was additionally supported under the auspices of the U.S. Department of Energy by Lawrence Livermore National Laboratory under contract DE-AC52-07NA27344. The statements, findings, conclusions, and recommendations do not necessarily reflect the views of these agencies. The paper's unique data product (LCT, shaded in Figure 5) may be obtained from the repository at http://weather.rsmas.miami.edu/repository/entry/show?entryid=30df8ea5-9e2e-4e90-af2b-a1f79f347586; please contact the lead author for questions and clarifications. MIMIC TPW data in Figure are available in our AMIE-DYNAMO field campaign archive at http://weather.rsmas.miami.edu/repository/entry/show?entryid=5c0355aa-bcc1-4b90-808f-48ecc03b7989. All other data are from readily accessible public repositories.

References

Ahmed, F., & Schumacher, C. (2015). Convective and stratiform components of the precipitation-moisture relationship. *Geophysical Research Letters*, *42*, 10,453–10,462. https://doi.org/10.1002/2015GL066957

Allen, M. R., & Ingram, W. J. (2002). Constraints on future changes in climate and the hydrologic cycle. *Nature*, *419*(6903), 224–232. https://doi.org/10.1038/nature01092

Allen, T. L., & Mapes, B. E. (2017). The late spring Caribbean rain-belt: climatology and dynamics. *International Journal of Climatology*, *37*, 4981–4993. https://doi.org/10.1002/joc.5136

Bretherton, C. S., Peters, M. E., & Back, L. E. (2004). Relationships between water vapor path and precipitation over the tropical oceans. *Journal of Climate*, *17*(7), 1517–1528. https://doi.org/10.1175/1520-0442(2004)017%3C1517:RBWVPA%3E2.0.CO;2

Chikira, M. (2014). Eastward-propagating intraseasonal oscillation represented by Chikira-Sugiyama cumulus parameterization. Part II: Understanding Moisture Variation under Weak Temperature Gradient Balance. *Journal of the Atmospheric Sciences*, *71*, 615–639.

Dee, D. P., Uppala, S. M., Simmons, A. J., Berrisford, P., Poli, P., Kobayashi, S., … Vitart, F. (2011). The ERA-Interim reanalysis: Configuration and performance of the data assimilation system. *Quarterly Journal of the Royal Meteorological Society*, *137*(656), 553–597. https://doi.org/10.1002/qj.828

Doswell, C. A. III, Brooks, H. E., & Maddox, R. A. (1996). Flash flood forecasting: An ingredients-based methodology. *Weather and Forecasting*, *11*(4), 560–581. https://doi.org/10.1175/1520-0434(1996)011%3C0560:FFFAIB%3E2.0.CO;2

Graham, N. E., & Barnett, T. P. (1987). Sea surface temperature, surface wind divergence, and convection over tropical oceans. *Science*, *238*(4827), 657–659. https://doi.org/10.1126/science.238.4827.657

Hannah, W. M., Mapes, B. E., & Elsaesser, G. S. (2016). A Lagrangian view of moisture dynamics during DYNAMO. *Journal of the Atmospheric Sciences*, *73*(5), 1967–1985. https://doi.org/10.1175/JAS-D-15-0243.1

Houze, R. A. Jr. (1997). Stratiform precipitation in regions of convection: A meteorological paradox? *Bulletin of the American Meteorological Society*, *78*(10), 2179–2196. https://doi.org/10.1175/1520-0477(1997)078%3C2179:SPIROC%3E2.0.CO;2

Houze, R. A. Jr. (2004). Mesoscale convective systems. *Reviews of Geophysics*, *42*. RG4003, doi:https://doi.org/10.1029/2004RG000150

Huffman, G. J., Bolvin, D. T., Nelkin, E. J., Wolff, D. B., Adler, R. F., Gu, G., … Stocker, E. F. (2007). The TRMM multisatellite precipitation analysis (TMPA): Quasi-global, multiyear, combined-sensor precipitation estimates at fine scales. *Journal of Hydrometeorology*, *8*(1), 38–55. https://doi.org/10.1175/JHM560.1

Johnson, N. C., & Xie, S.-P. (2010). Changes in the sea surface temperature threshold for tropical convection. *Nature Geoscience*, *3*, 842–845.

Kim, D., Xavier, P., Maloney, E., Wheeler, M., Waliser, D., Sperber, K., … Liu, H. (2014). Process-oriented MJO simulation diagnostic: Moisture sensitivity of simulated convection. *Journal of Climate*, *27*(14), 5379–5395. https://doi.org/10.1175/JCLI-D-13-00497.1

Knippertz, P., Wernli, H., & Gläser, G. (2013). A global climatology of tropical moisture exports. *Journal of Climate*, *26*(10), 3031–3045. https://doi.org/10.1175/JCLI-D-12-00401.1

Mapes, B. E. (2001). Water's two height scales: The moist adiabat and the radiative troposphere. *Quarterly Journal of the Royal Meteorological Society*, *127*(577), 2353–2366. https://doi.org/10.1002/qj.49712757708

Marchand, R., Mace, G. G., Ackerman, T., & Stephens, G. (2008). Hydrometeor detection using Cloudsat—An Earth-orbiting 94-GHz cloud radar. *Journal of Atmospheric and Oceanic Technology*, *25*(4), 519–533. https://doi.org/10.1175/2007JTECHA1006.1

Neelin, J. D., Peters, O., & Hales, K. (2009). The transition to strong convection. *Journal of the Atmospheric Sciences*, *66*(8), 2367–2384. https://doi.org/10.1175/2009JAS2962.1

Peters, O., & Neelin, J. D. (2006). Critical phenomena in atmospheric precipitation. *Nature Physics*, *2*(6), 393–396. https://doi.org/10.1038/nphys314

Raymond, D. J., Sessions, S. L., Sobel, A. H., & Fuchs, Z. (2009). The mechanics of gross moist stability. *Journal of Advances in Modeling Earth Systems*, *1*(3), 9. https://doi.org/10.3894/JAMES.2009.1.9

Schiro, K. A., Neelin, J. D., Adams, D. K., & Lintner, B. R. (2016). Deep convection and column water vapor over tropical land versus tropical ocean: A comparison between the Amazon and the tropical western Pacific. *Journal of the Atmospheric Sciences*, *73*(10), 4043–4063. https://doi.org/10.1175/JAS-D-16-0119.1

Schultz, D. M., Schumacher, P. N., & Doswell, C. A. III (2000). The intricacies of instabilities. *Monthly Weather Review*, *128*(12), 4143–4148. https://doi.org/10.1175/1520-0493(2000)129%3C4143:TIOI%3E2.0.CO;2

Seidel, D. J., Fu, Q., Randel, W. J., & Reichler, T. J. (2007). Widening of the tropical belt in a changing climate. *Nature Geoscience*, *1*(1), 21–24. https://doi.org/10.1038/ngeo.2007.38

Sherwood, S. C., Roca, R., Weckwerth, T. M., & Andronova, N. G. (2010). Tropospheric water vapor, convection, and climate. *Reviews of Geophysics*, *48*, RG2001. https://doi.org/10.1029/2009RG000301

Shields, C. A., & Kiehl, J. T. (2016). Atmospheric river landfall-latitude changes in future climate simulations. *Geophysical Research Letters*, *43*, 8775–8782. https://doi.org/10.1002/2016GL070470

Stephens, G. L., Vane, D. G., Boain, R. J., Mace, G. G., Sassen, K., Wang, Z., … Mitrescu, C. (2002). The Cloudsat mission and the A-Train. A new dimension of space-based observations of clouds and precipitation. *Bulletin of the American Meteorological Society*, *83*, 1771–1790. https://doi.org/10.1175/BAMS-83-12-1771

Stevens, B. (2005). Atmospheric moist convection. *Annual Review of Earth and Planetary Sciences*, *33*(1), 605–643. https://doi.org/10.1146/annurev.earth.33.092203.122658

Taylor, K. E., Stouffer, R. J., & Meehl, G. A. (2012). An overview of CMIP5 and the experiment design. *Bulletin of the American Meteorological Society*, *93*(4), 485–498. https://doi.org/10.1175/BAMS-D-11-00094.1

Wimmers, A. J., & Velden, C. S. (2011). Seamless advective blending of total precipitable water retrievals from polar-orbiting satellites. *Journal of Applied Meteorology and Climatology*, *50*(5), 1024–1036. https://doi.org/10.1175/2010JAMC2589.1

Zhang, C., Mapes, B. E., & Soden, B. J. (2003). Bimodality in tropical water vapour. *Quarterly Journal of the Royal Meteorological Society*, *129*(594), 2847–2866. https://doi.org/10.1256/qj.02.166

Zhang, C., Nolan, D. S., Thorncroft, C. D., & Nguyen, H. (2008). Shallow meridional circulation in the tropical atmosphere. *Journal of Climate*, *21*(14), 3453–3470. https://doi.org/10.1175/2007JCLI1870.1